Non-searching High Speed Target Detection Method for Carrier Frequency and Pulse Repetition Frequency Agile Radar

Wenchao YU, Weimin SU, Hong GU

School of Electronic and Optical Engineering, Nanjing University of Science and Technology, Nanjing, China

wenchao968@163.com

Submitted December 26, 2025 / Accepted April 24, 2026 / Online first April 28, 2026

Abstract. *Range migration has become the major problem faced by radar high speed target detection. The existing methods primarily focus on range migration elimination and coherent integration in the traditional radar system with fixed carrier frequency (CF) and pulse repetition frequency (PRF), whereas they are not applicable to the radar system with joint agility of CF and PRF, which possesses robust low probability of intercept (LPI) and anti-jamming performance under complex electromagnetic circumstances. In this paper, the high speed target detection problem for the CF-PRF agile radar system is considered and a non-searching coherent integration algorithm is proposed, where range frequency reversal and correlation transform (RFRCT), azimuth nonuniform fast Fourier transform (NUFFT) and range inverse fast Fourier transform (IFFT) are combined to eliminate the effect of range migration and radar parameter agility upon coherent integration. Experimental results have been provided to validate the effectiveness of the proposed method.*

Keywords

High speed target, Carrier Frequency (CF) and Pulse Repetition Frequency (PRF) agile radar, range migration, coherent integration, target detection

1. Introduction

With the rapid development of aerospace technology, a growing number of high-speed targets have appeared in the field of radar detection [1–3]. Prolonging the observation time is conducive to improving radar detection capability for weak targets, whereas the target's high speed motion will cause range migration and disperse the echo energy across multiple range cells, which will render the traditional moving target detection (MTD) method ineffective [4–6].

In order to compensate the effect of range migration, various incoherent and coherent algorithms have been proposed in the existing literatures. As typical incoherent methods, Hough transform [7–9] and Radon transform [10–12] accumulate the target's energy along the motion trajectory. Although straightforward to implement, these algorithms discard the signal phase information and are vulnerable to noise effect. Compared with incoherent methods, the existing coherent integration algorithms exhibit superior energy accumulation performance, such as Keystone transform (KT) and Radon Fourier transform (RFT). Aiming at eliminating range migration via decoupling the range frequency and slow time variables, KT rescales the slow time axis and can be fast implemented via chirp-z transform [13–18]. However, KT will become invalid when Doppler ambiguity occurs. As a modified form of Radon transform, Radon Fourier transform (RFT) performs the 2-D search for range and velocity to extract the target's motion trajectory, then conducts Doppler filtering to coherently accumulate echo energy [19–21]. What's more, some other coherent integration methods, e.g., axis rotation MTD [22], [23] and segmented RFT [24], have also been proposed to fulfill high speed target detection. In order to reduce parameter search and improve the real-time performance, some nonlinear methods have also been proposed, such as sequence reversing transform (SRT) [25] and range frequency polynomial phase transform (RFPPT) [26].

While capable of achieving range migration compensation, the aforementioned algorithms are only applicable to traditional radar system with fixed carrier frequency (CF) and pulse repetition frequency (PRF). With the development of electronic countermeasures technology, radar CF or PRF agility has become a common anti-jamming strategy, which can reduce the interception and recognition probabilities of radar waveform. With respect to signal processing in the parameter-agile radar system, several algorithms have been presented to realize coherent integration and high speed target detection. The Radon-nonuniform fast Fourier transform (NUFFT) method extracts the target trajectory via Radon transform, then compensates the phase fluctuation caused by CF agility via NUFFT [27]. In consideration of PRF agility, the random pulse repetition interval (RPRI)-RFT algorithm extends the

DOI: 10.13164/re.2026.0247

signal processing framework of RFT to the random PRF radar system, thereby enabling range migration compensation and high speed target detection [28], [29]. Although Radon-NUFFT and RPRI-RFT take into account the scenario of radar parameter agility, they both require a 2-D parameter search with heavy computational burden. Furthermore, they are unable to accommodate CF-PRF dual agility, which achieves better low probability of intercept (LPI) and anti-jamming performance than single parameter agility, due to the introduction of randomness in both carrier frequency and pulse emission timing. For the sake of solving this problem, we propose a non-searching high speed target detection algorithm for CF-PRF agile radar in this paper. The proposed method firstly conducts range frequency reversal and correlation transform (RFRCT) to remove the phase term with respect to CF agility, then adopts azimuth NUFFT and range inverse fast Fourier transform (IFFT) to eliminate the effect of range migration and PRF agility upon coherent integration. The theoretical analysis and experimental results are provided to validate the high efficiency and effectiveness of the proposed method.

The rest of this paper is organized as follows. Section 2 establishes the signal model. Section 3 introduces the proposed method in the single target and multi-target detection environments. In Sec. 4, the computational complexity of the proposed method is analyzed. Section 5 provides the experimental results and detection performance analysis. Lastly, the conclusions are given in Sec. 6.

2. Signal Model

The transmitted signal of the CF-PRF agile radar can be expressed as

$$s_t\left(t_m,t\right)=\mathrm{rect}\left(\frac{t}{T_\mathrm{p}}\right)\exp\left[\mathrm{j}2\pi f_{\mathrm{c},m}\left(t_m+t\right)\right]\exp\left(\mathrm{j}\pi\mu t^2\right) \tag{1}$$

where t_m and t denote the slow time and fast time variables, respectively. $m\in[1,2,\ldots,M]$ denotes the pulse index, rect(·), M, T_p and μ represent the rectangle window function, total number of pulses, pulse width and chirp rate, respectively. $f_{\mathrm{c},m}=f_{\mathrm{c}0}+\Delta f_{\mathrm{c},m}$ denotes the CF of the mth pulse, where $f_{\mathrm{c}0}$ is the center CF, $\Delta f_{\mathrm{c},m}$ is the CF jitter which is randomly distributed within $[-B_\mathrm{CF}/2, B_\mathrm{CF}/2]$, B_CF is the CF agility bandwidth. Similarly, define $f_{\mathrm{r},m}=f_{\mathrm{r}0}+\Delta f_{\mathrm{r},m}$ as the PRF of the mth pulse, where $f_{\mathrm{r}0}$, $\Delta f_{\mathrm{r},m}\in[-B_\mathrm{PRF}/2, B_\mathrm{PRF}/2]$, B_PRF denote the center PRF, PRF jitter and agility bandwidth, respectively. Then, the slow time axis can be obtained by

$$t_m=\begin{cases}0, & m=1\\ \sum_{i=1}^{m-1}1/\,f_{\mathrm{r},i}, & m\in[2,\,3,\,\cdots,\,M]\end{cases} \tag{2}$$

The received signal for the high-speed target can be modeled by

$$\begin{aligned}s_r\left(t_m,t\right)=\sigma\mathrm{rect}&\left[\frac{t-2R(t_m)/c}{T_\mathrm{p}}\right]\exp\left[\mathrm{j}\pi\mu\left(t-\frac{2R(t_m)}{c}\right)^2\right]\\&\times\exp\left[-\mathrm{j}\frac{4\pi}{c}f_{\mathrm{c},m}R\left(t_m\right)\right]\end{aligned} \tag{3}$$

where σ and c denote the target reflectively and light speed, respectively. $R(t_m)=\mathrm{r}+vt_m$ is the instantaneous slant range from radar to target, r and v denote the initial slant range and radial velocity of the target, respectively.

After performing pulse compression, the compressed signal in the range frequency domain can be expressed as

$$\begin{aligned}S(t_m,f)&=A_1\mathrm{rect}\left(\frac{f}{B}\right)\exp\left[-\mathrm{j}\frac{4\pi}{c}\left(f+f_{\mathrm{c},m}\right)\left(r+vt_m\right)\right]\\&=A_1\mathrm{rect}\left(\frac{f}{B}\right)\underbrace{\exp\left(-\mathrm{j}\frac{4\pi}{c}fr\right)}_{\Phi_1}\underbrace{\exp\left(-\mathrm{j}\frac{4\pi}{c}f_{\mathrm{c},m}r\right)}_{\Phi_2}\\&\quad\times\underbrace{\exp\left(-\mathrm{j}\frac{4\pi}{c}fvt_m\right)}_{\Phi_3}\underbrace{\exp\left(-\mathrm{j}\frac{4\pi}{c}f_{\mathrm{c},m}vt_m\right)}_{\Phi_4}\end{aligned} \tag{4}$$

where f, A_1 and B represent the range frequency variable, signal amplitude and bandwidth, respectively.

In (4), Φ_1 is the range phase term with respect to f, Φ_2 is the range phase fluctuation due to CF agility, Φ_3 is the range migration phase caused by the coupling between f and t_m, and Φ_4 is the Doppler phase fluctuation due to the joint agility of CF and PRF. Clearly, the range migration correction and jittered phase compensation are the two problems faced by high speed target detection in the CF-PRF agile radar system.

3. Proposed Method

3.1 Coherent Integration for Single Target Detection

Considering the symmetrical property of the range frequency axis, we can obtain the reversed frequency variable as below

$$\begin{aligned}\bar{f}&=-f\\&=\frac{f_\mathrm{s}}{2},\frac{f_\mathrm{s}}{2}-\frac{f_\mathrm{s}}{N},\cdots,-\frac{f_\mathrm{s}}{2}+\frac{f_\mathrm{s}}{N}\end{aligned} \tag{5}$$

where f_s and N represent the sampling rate and the number of range sampling points, respectively.

Substituting (5) into (4), the range compressed signal with frequency reversal can be constructed as

$$S(t_m,\overleftarrow{f}) = A_1\mathrm{rect}\left(\frac{\overleftarrow{f}}{B}\right)\exp\left[-\mathrm{j}\frac{4\pi}{c}\left(\overleftarrow{f}+f_{\mathrm{c},m}\right)\left(r+vt_m\right)\right] = A_1\mathrm{rect}\left(\frac{f}{B}\right)\exp\left[-\mathrm{j}\frac{4\pi}{c}\left(f_{\mathrm{c},m}-f\right)\left(r+vt_m\right)\right]. \quad (6)$$

For the purpose of removing the phase fluctuation caused by CF agility, define the frequency shift Δf and perform the correlation processing as below

$$\begin{aligned} S_{\mathrm{c}}(t_m,f) &= S(t_m,f)S^*(t_m,\overleftarrow{f}-\Delta f) \\ &= A_1^2\mathrm{rect}\left(\frac{f}{B-\Delta f}\right)\exp\left[-\mathrm{j}\frac{8\pi}{c}\left(f+\frac{\Delta f}{2}\right)\left(r+vt_m\right)\right] \\ &= A_2\mathrm{rect}\left(\frac{f}{B-\Delta f}\right)\exp\left(-\mathrm{j}\frac{8\pi}{c}fr\right)\exp\left(\mathrm{j}2\pi\Delta f_{\mathrm{d}}\xi t_m\right) \end{aligned} \quad (7)$$

where $A_2 = A_1^2\exp(-\mathrm{j}4\pi\Delta fr/c)$ is the signal complex amplitude, $\Delta f_{\mathrm{d}} = -2v\Delta f/c$ is the equivalent Doppler shift of the high speed target, and $\xi = 1 + 2f/\Delta f$.

Comparing (7) with the pulse compressed signal in (4), it can be seen that the agile CF has been converted from $f_{\mathrm{c},m}$ to a fixed equivalent CF Δf, which indicates the elimination of CF agility, whereas the coupling between f and t_m still exists which will lead to range migration. Here, the azimuth Fourier transform (FT) is conducted to solve the problem, which is formulated as

$$\begin{aligned} R(f_m,f) &= \int S_{\mathrm{c}}(t_m,f)\exp\left(-\mathrm{j}2\pi f_m\xi t_m\right)\mathrm{d}\xi t_m \\ &= A_3\mathrm{rect}\left(\frac{f}{B-\Delta f}\right)\exp\left(-\mathrm{j}\frac{8\pi}{c}fr\right)\delta\left(f_m-\Delta f_{\mathrm{d}}\right) \end{aligned} \quad (8)$$

where f_m and A_3 denote the azimuth frequency variable and signal amplitude, respectively.

In (8), it is noted that due to PRF agility, the slow time axis of $S_{\mathrm{c}}(t_m, f)$ is non-uniformly sampled and the azimuth FT cannot be fast implemented via FFT. In order to map the non-equidistant slow time grids to the equidistant azimuth frequency grids efficiently, NUFFT is adopted to resample the slow time axis and realize azimuth FT [30–32].

Let $S_{\mathrm{c}}(m, n)$ and $R(m, n)$ represent the discrete form of $S_{\mathrm{c}}(t_m, f)$ and $R(f_m, f)$, respectively. Then, azimuth NUFFT is conducted via the following three steps:

Step 1: Grid interpolation

$$u\left(\mu_m^{(n)}+l,n\right) = \sum_{m=1}^{M}\sum_{l=-L}^{L}\frac{1}{\sqrt{2\pi}}\hat{\phi}\left(\gamma x_m^{(n)}-\mu_m^{(n)}-l\right)S_{\mathrm{c}}(m,n) \quad (9)$$

where $x_m^{(n)}$ denotes the non-uniform sampling grid corresponding to $S_{\mathrm{c}}(m, n)$, $\mu_m^{(n)}$ denotes the nearest integer to $\gamma x_m^{(n)}$. γ and L represent the oversampling factor and interpolation length, respectively.

Step 2: Compute the azimuth FFT of size γM

$$U(m,n) = \sum_{k=-\gamma M/2}^{\gamma M/2-1}u(k,n)\exp\left(-\mathrm{j}\frac{2\pi mk}{\gamma M}\right). \quad (10)$$

Step 3: Obtain the result via azimuth scaling

$$R(m,n) = \frac{U(m,n)}{\phi(m)},\quad m=-M/2,\cdots,M/2-1. \quad (11)$$

It is noted that in (9) and (11), $\hat{\phi}(\cdot)$ and $\phi(\cdot)$ denote the time and frequency forms of Kaiser-Bessel window, respectively. After conducting azimuth NUFFT, range IFFT can be performed to obtain the final coherent integration result, i.e.,

$$\begin{aligned} G(f_m,t) &= \underset{f}{\mathrm{IFFT}}\left[R(f_m,f)\right] \\ &= \int R(f_m,f)\exp\left(\mathrm{j}2\pi ft\right)\mathrm{d}f \\ &= A_4\mathrm{sinc}\left[\left(B-\Delta f\right)\left(t-\frac{4r}{c}\right)\right]\delta\left(f_m-\Delta f_{\mathrm{d}}\right) \end{aligned} \quad (12)$$

where A_4 denotes the signal amplitude.

It can be noticed from (12) that after coherent integration, the target energy can be accumulated as a peak in the range-Doppler domain, then the constant false-alarm rate (CFAR) detector can be conducted to determine the presence or absence of a target, i.e., $|G(f_m,t)| \underset{\mathrm{H}_0}{\overset{\mathrm{H}_1}{\gtrless}} \eta_{\mathrm{T}}$, where η_{T} denotes the adaptive detection threshold. When the test statistic is higher than the threshold, the hypothesis H_1 is used to indicate the presence of a target, otherwise the hypothesis H_0 is used to indicate the absence of a target.

3.2 Coherent Integration for Multi-Target Detection

In the above analysis, the scenario of single target detection is considered and the efficient coherent integration algorithm which combines RFRCT, azimuth NUFFT and range IFFT is proposed. However, multiple targets might coexist in practical applications and it is necessary to consider the coherent integration for multi-target detection. Suppose that the number of targets is K, the range compressed signal in (4) can be reformulated as

$$S(t_m,f) = \sum_{i=1}^{K}A_{1,i}\mathrm{rect}\left(\frac{f}{B}\right)\exp\left[-\mathrm{j}\frac{4\pi}{c}\left(f+f_{\mathrm{c},m}\right)\left(r_i+v_it_m\right)\right] \quad (13)$$

where $A_{1,i}$, r_i and v_i represent the signal amplitude, initial slant range and radial velocity of the ith target, respectively.

Performing RFRCT upon $S(t_m, f)$, we obtain

$$S_{\mathrm{c}}(t_m,f) = S_{\mathrm{c,self}}(t_m,f) + S_{\mathrm{c,cross}}(t_m,f). \quad (14)$$

In (14), $S_{\mathrm{c,\,self}}(t_m, f)$ and $S_{\mathrm{c,\,cross}}(t_m, f)$ represent the self terms and cross terms, respectively, i.e.,

$$S_{\text{c,self}}(t_m, f) = \sum_{i=1}^{K} A_{2,i}\,\text{rect}\left(\frac{f}{B-\Delta f}\right)\exp\left(-\text{j}\frac{8\pi}{c} f r_i\right) \times \exp\left(\text{j}2\pi\Delta f_{\text{d},i}\xi t_m\right) \quad (15)$$

where $A_{2,i} = A_{1,i}^2 \exp\left(-\text{j}4\pi\Delta f r_i / c\right)$ and $\Delta f_{\text{d},i} = -2v_i\Delta f / c$.

$$S_{\text{c,cross}}(t_m, f) = \sum_{i=1}^{K}\sum_{j=1, j\neq i}^{K} A_{2,ij}\,\text{rect}\left(\frac{f}{B-\Delta f}\right)\exp\left[-\text{j}\frac{4\pi}{c} f\left(r_i + r_j\right)\right] \times \exp\left[-\text{j}\frac{4\pi}{c} f\left(v_i + v_j\right)t_m\right]\exp\left(-\text{j}\frac{4\pi}{c}\Delta f v_j t_m\right) \times \exp\left\{-\text{j}\frac{4\pi}{c} f_{\text{c},m}\left[\left(r_i - r_j\right) + \left(v_i - v_j\right)t_m\right]\right\} \quad (16)$$

where $A_{2,ij} = A_{1,i}A_{1,j}\exp\left(-\text{j}4\pi\Delta f r_j / c\right)$.

From (14) to (16), it can be seen that the fluctuating phase due to CF agility for each self term has been eliminated, thus each target can be well focused via the subsequent azimuth NUFFT and range IFFT operations. As for the cross terms, due to the situation that $r_i \neq r_j$ or $v_i \neq v_j$ for different targets, the phase term with respect to $f_{\text{c},m}$ still exists after conducting RFRCT, and the signal structure is mismatched with the azimuth FT operator defined in (8), hence the energy of cross terms will be suppressed for the final output in the range-Doppler domain.

The flowchart of the proposed method is shown in Fig. 1.

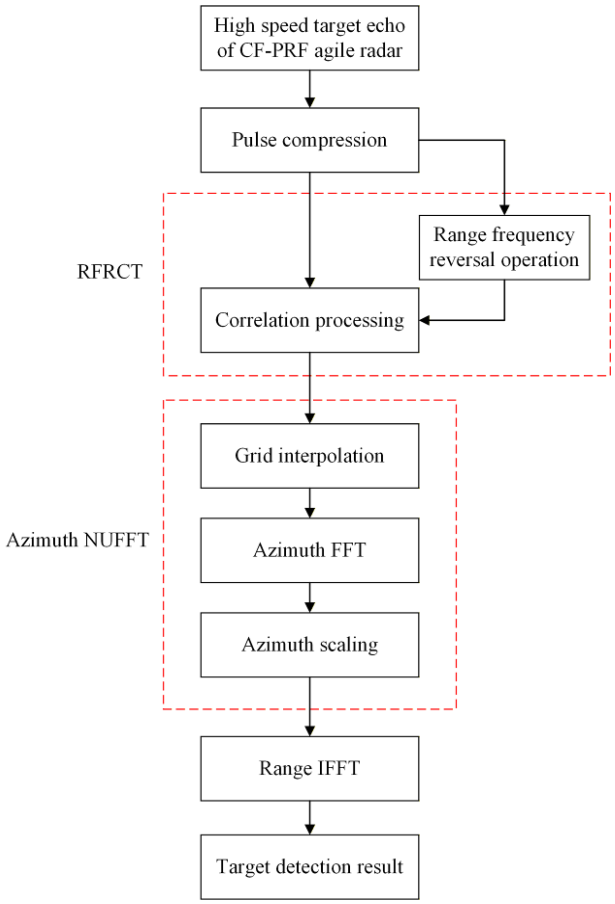

Fig. 1. Flowchart of the proposed method.

4. Computational Complexity Analysis

In what follows, the computational complexity of the proposed method is analyzed and compared with Radon-NUFFT, RPRI-RFT, SRT and RFPPT, in terms of the number of complex multiplications. Denote that M and N represent the number of echo pulses and range cells, respectively.

For the proposed method, the RFRCT operation needs a 2-D complex multiplication with the computational cost of $O(MN)$. Subsequently, the azimuth NUFFT is conducted via signal interpolation, FFT and scaling, with the computational cost of $O(2LMN)$, $O(\gamma MN / 2 \times \log_2 \gamma M)$, and $O(MN)$, respectively. Lastly, range IFFT is performed with computational cost of $O(MN / 2 \times \log_2 N)$. Hence, the total computational complexity of the proposed algorithm is $O(MN(2 + 2L + \gamma / 2 \times \log_2 \gamma M + 1/2 \times \log_2 N))$.

Denote the number of search range and search velocity as N_r and N_v, respectively. For Radon-NUFFT, the phase compensation with respective to range-agile frequency is conducted with the computational cost of $O(MN)$. Then, the 2-D joint search for the target's initial slant range and radial velocity is performed. In each search, the phase compensation for Doppler frequency ambiguity is needed, then NUFFT is utilized to realize coherent integration, where the computational complexities are $O(M)$ and

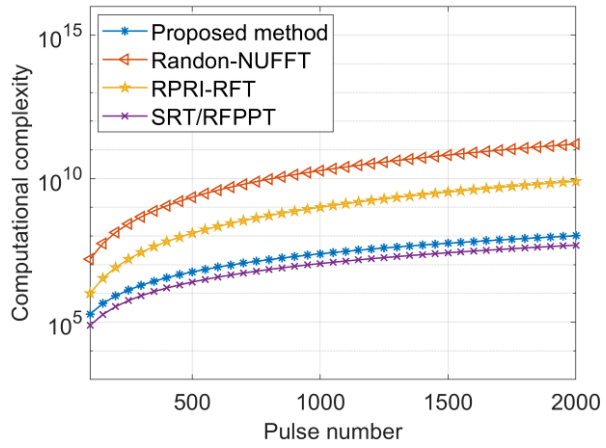

Fig. 2. Computational complexity curves of different methods.

$O(M(2L + \gamma/2 \times \log_2 \gamma M + 1))$, respectively. Hence, the total computational complexity of Radon-NUFFT is $O[MN + N_\text{r}N_\text{v}M\,(2 + 2L + \gamma / 2 \times \log_2 \gamma M)]$. As for RPRI-RFT, the 2-D joint search is also needed with the computational cost of $O(MN_\text{r}N_\text{v})$.

As for SRT and RFPPT, the 2-D matrix multiplication, range IFFT, and azimuth FFT operations are both needed, with the computational cost of $O(MN)$, $O(MN / 2 \times \log_2 N)$ and $O(MN / 2 \times \log_2 M)$, respectively. Thus, the total computational cost of SRT and RFPPT are both $O(MN(1 + 1/2 \times \log_2 N + 1/2 \times \log_2 M))$.

The oversampling factor and interpolation length in NUFFT are set as their typical values. i.e., $\gamma = 2$ and $L = 3$, respectively [31]. Under the assumption that $M = N = N_r = N_v$, Figure 2 shows the computational complexity curves versus pulse number of the proposed method, Radon-NUFFT, RPRI-RFT, SRT and RFPPT. It can be seen that the computational cost of the proposed method is slightly higher than SRT and RFPPT, and is significantly lower than Radon-NUFFT and RPRI-RFT thanks to the non-searching mechanism.

5. Experimental Results

5.1 Single Target Detection

In this section, the coherent integration and detection performance of the proposed method is evaluated via several experimental results. Table 1 lists the radar system parameters. The initial slant range and radial velocity of the target are set as 20 km and 500 m/s, respectively. Considering the additive white Gaussian noise background with the signal-to-noise ratio (SNR) set as –8 dB

Parameter	Value
Center CF	6 GHz
Center PRF	2000 Hz
Signal bandwidth	10 MHz
Sampling frequency	12 MHz
Pulse width	50 μs
Integration time	0.5 s

Tab. 1. Radar system parameters.

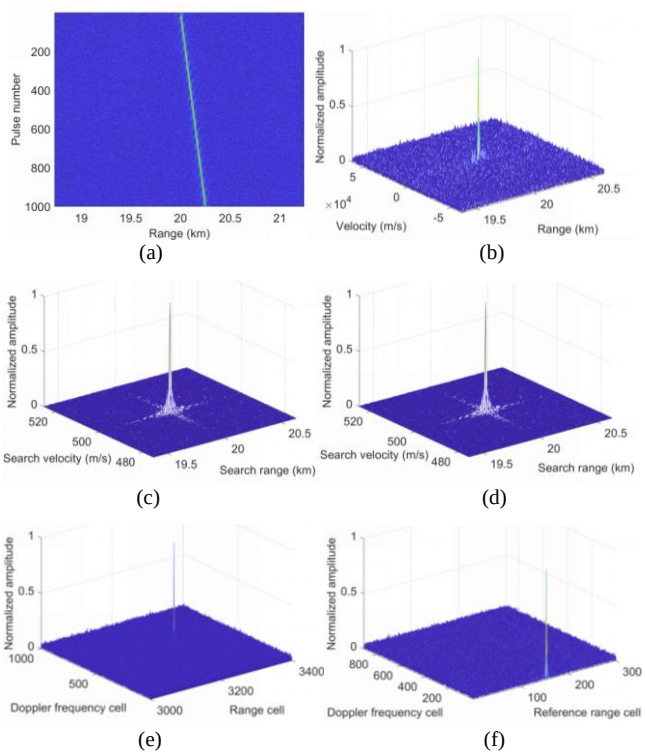

Fig. 3. Experimental results for single target detection with constant CF and constant PRF. (a) Target's motion trajectory after pulse compression. (b) Processed result of the proposed method. (c) Processed result of Radon-NUFFT. (d) Processed result of RPRI-RFT. (e) Processed result of SRT. (f) Processed result of RFPPT.

5.1.1 Single Target Detection with Constant CF and Constant PRF

In the scenario of single target detection with constant CF and constant PRF, Figure 3(a) depicts the target's motion trajectory after pulse compression, where severe range migration caused by the target's high speed movement can be observed. Figures 3(b)–(f) draw the processed results of the proposed method, Radon-NUFFT, RPRI-RFT, SRT and RFPPT, respectively. It can be seen that all the algorithms can overcome the effect of range migration and accumulate the target's energy.

5.1.2 Single Target Detection with Agile CF and Constant PRF

In the scenario of single target detection with agile CF and constant PRF, where the CF agility bandwidth is set as

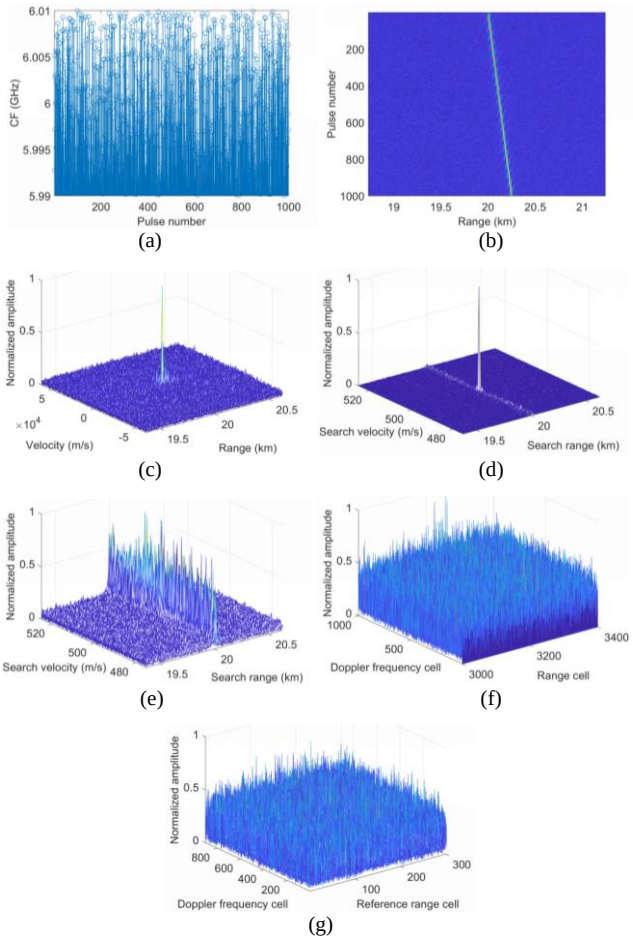

Fig. 4. Experimental results for single target detection with agile CF and constant PRF. (a) Agile CF sequence. (b) Target's motion trajectory after pulse compression. (c) Processed result of the proposed method. (d) Processed result of Radon-NUFFT. (e) Processed result of RPRI-RFT. (f) Processed result of SRT. (g) Processed result of RFPPT.

20 MHz. Figure 4(a) shows the agile CF sequences versus pulse number. Figure 4(b) depicts the target's motion trajectory after pulse compression. Figures 4(c)–(g) draw the processed results of the proposed method, Radon-NUFFT, RPRI-RFT, SRT and RFPPT, respectively. It can be observed that both the proposed method and Radon-NUFFT exhibit robustness to CF agility, while other algorithms suffer from significant performance degradation.

5.1.3 Single Target Detection with Constant CF and Agile PRF

In the scenario of single target detection with constant CF and agile PRF, where the PRF agility bandwidth is set as 200 Hz. Figure 5(a) shows the agile CF sequences versus pulse number. Figure 5(b) depicts the target's motion trajectory after pulse compression. Figures 5(c)–(g) draw the processed results of the proposed method, Radon-NUFFT, RPRI-RFT, SRT and RFPPT, respectively. Evidently, both the proposed method and RPRI-RFT are robust against PRF agility, in contrast to other algorithms that experience performance deterioration.

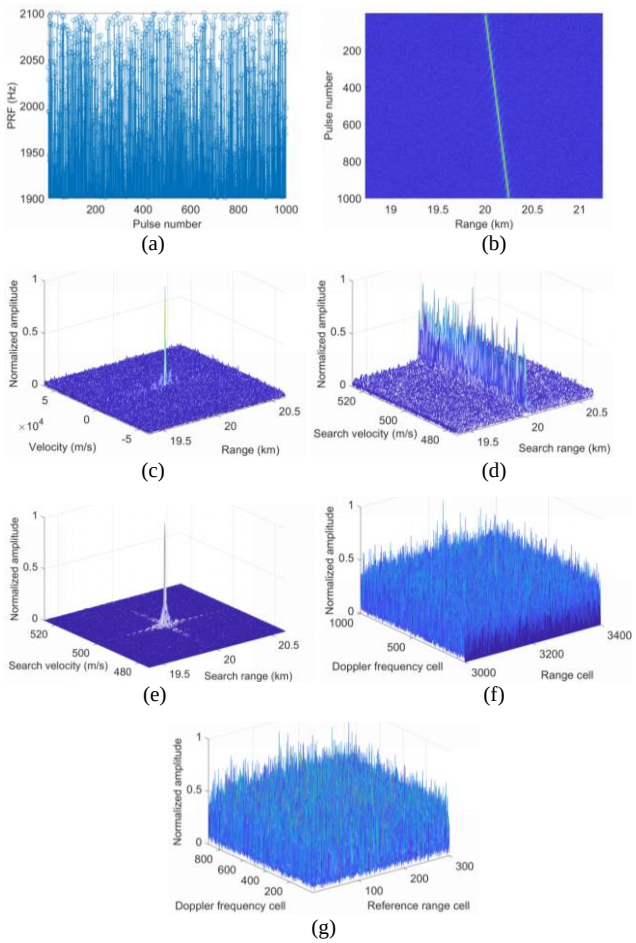

Fig. 5. Experimental results for single target detection with constant CF and agile PRF. (a) Agile PRF sequence. (b) Target's motion trajectory after pulse compression. (c) Processed result of the proposed method. (d) Processed result of Radon-NUFFT. (e) Processed result of RPRI-RFT. (f) Processed result of SRT. (g) Processed result of RFPPT.

5.1.4 Single Target Detection with Agile CF and Agile PRF

In the scenario of single target detection with agile CF and agile PRF, where the CF agility bandwidth and PRF agility bandwidth are set as 20 MHz and 200 Hz, respectively. Figures 6(a) and (b) show the agile CF and PRF sequences versus pulse number, respectively. Figure 6(c) depicts the target's motion trajectory after pulse compression. Figures 6(d)–(h) draw the processed results of the proposed method, Radon-NUFFT, RPRI-RFT, SRT and RFPPT, respectively. It can be noticed that under the circumstance of CF-PRF dual agility, the proposed method can still accumulate the target's echo energy thanks to the adoption of RFRCT and azimuth NUFFT, while other algorithm exhibit poor accumulation performance.

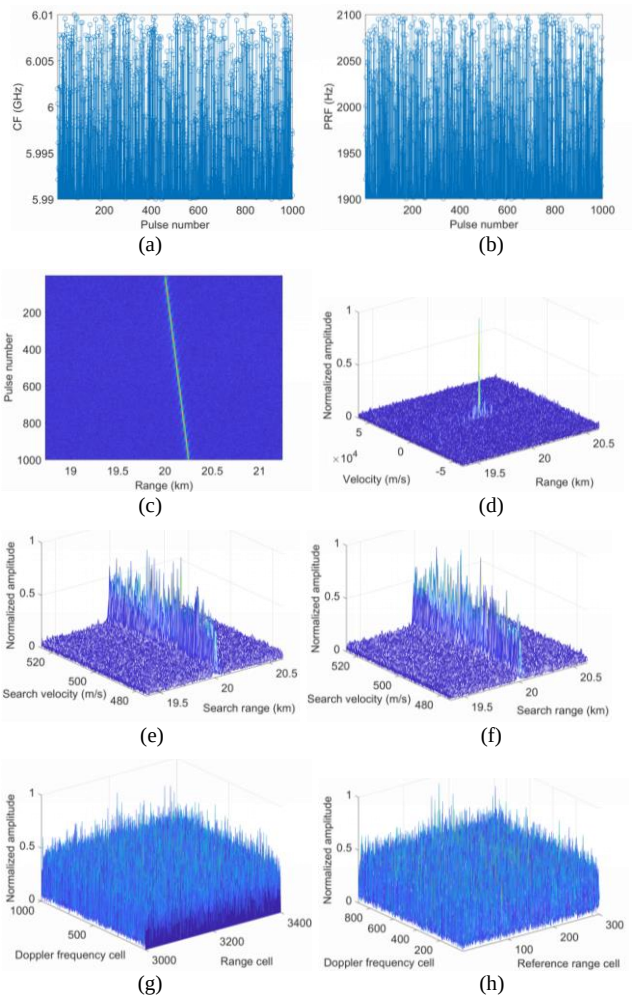

Fig. 6. Experimental results for single target detection with agile CF and agile PRF. (a) Agile CF sequence. (b) Agile PRF sequence. (c) Target's motion trajectory after pulse compression. (d) Processed result of the proposed method. (e) Processed result of Radon-NUFFT. (f) Processed result of RPRI-RFT. (g) Processed result of SRT. (h) Processed result of RFPPT.

Parameter	Target 1	Target 2
Initial slant range	20 km	20.2 km
Radial velocity	500 m/s	–500 m/s

Tab. 2. Target parameters.

5.2 Multi-Target Detection with Agile CF and Agile PRF

In order to evaluate the detection performance of the proposed method in the multi-target environment, the mixed echo of two high speed targets is generated and processed. The radar system parameters are listed in Tab. 1. The CF agility bandwidth and PRF agility bandwidth are set as 20 MHz and 200 Hz, respectively. The initial slant ranges and radial velocities of target 1 and 2 are listed in Tab. 2. Figure 7(a) depicts the motion trajectories of the two targets after pulse compression. Figures 7(b)–(f) draw the processed results of the proposed method, Radon-NUFFT, RPRI-RFT, SRT and RFPPT, respectively. Obviously, the proposed algorithm is capable of suppressing cross terms and accumulating the self term of each target, while other methods fail to detect any target.

5.3 Detection Performance Analysis

In what follows, the detection performance of the proposed method is analyzed and compared with Radon-NUFFT, RPRI-RFT, SRT, RFPPT and MTD, where the methods are applied under the conditions for which they were originally intended. Setting the false alarm probability of CFAR detector as 10^{-6}, Figure 8 depicts the detection probability curves of different methods, where 500 Monte Carlo experiments are conducted for each SNR stage from

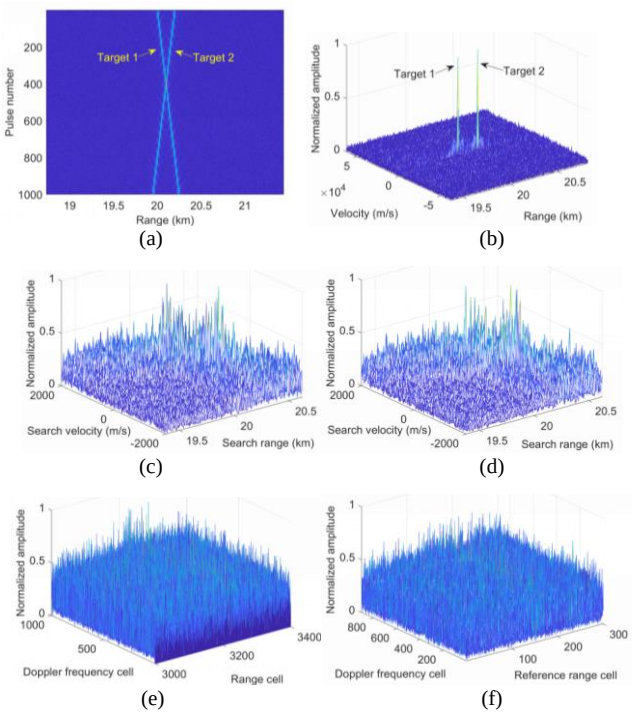

Fig. 7. Experimental results for multi-target detection with agile CF and agile PRF. (a) Motion trajectories of the two targets after pulse compression. (b) Processed result of the proposed method. (c) Processed result of Radon-NUFFT. (d) Processed result of RPRI-RFT. (e) Processed result of SRT. (f) Processed result of RFPPT.

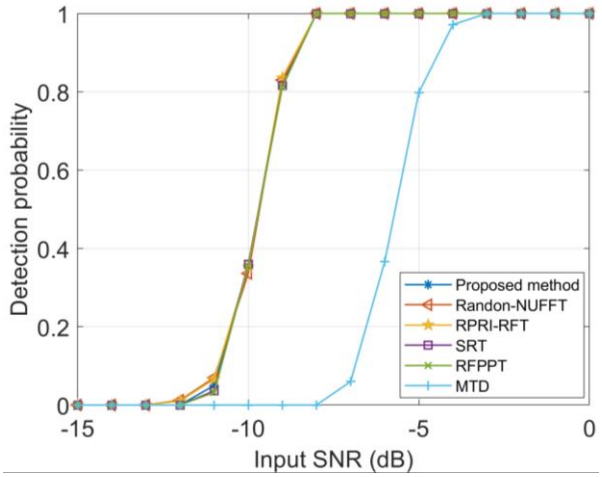

Fig. 8. Detection probability comparison among different methods for high speed target detection.

–15 dB to 0 dB. It can be noticed that the detection performance of the proposed algorithm follows that of Radon-NUFFT, RPRI-RFT, SRT and RFPPT. As for MTD, the range migration of the target echo cannot be eliminated, which deteriorates the detection performance.

6. Conclusions

In this paper, we propose a non-searching high speed target detection method for the CF-PRF agile radar system, where RFRCT, azimuth NUFFT and range IFFT are combined to compensate range migration and fluctuating phase terms with high efficiency. Compared with Radon-NUFFT and RPRI-RFT which only consider single parameter agility, the proposed algorithm further considers CF-PRF dual agility, thereby achieving superior LPI and anti-jamming performance. Furthermore, a lower computational cost is obtained due to the avoidance of 2-D parameter search. Experimental results have been provided to validate the effectiveness of the proposed algorithm in the environments of both single target and multi-target detection.

Acknowledgments

This work was supported in part by the Natural Science Foundation of Jiangsu Province under Grant BK20230915.

References

[1] SUN, Z., LI, X., YI, W., et al. A coherent detection and velocity estimation algorithm for the high-speed target based on the modified location rotation transform. *IEEE Journal of Selected Topics in Applied Earth Observations and Remote Sensing*, 2018, vol. 11, no. 7, p. 2346–2361. DOI: 10.1109/JSTARS.2018.2834535

[2] WANG, M., LI, X., ZHANG, Z., et al. Coherent integration and parameter estimation for high-speed target detection with bistatic MIMO radar. *IEEE Transactions on Geoscience and Remote Sensing*, 2023, vol. 61, p. 1–15. DOI: 10.1109/TGRS.2023.3298825

[3] YU, W., LU, X., SU, W., et al. Efficient long-time coherent integration and detection algorithm for radar high-speed target based on the azimuth resampling technology. *IEEE Transactions on Aerospace and Electronic Systems*, 2024, vol. 60, no. 1, p. 1091–1101. DOI: 10.1109/TAES.2023.3334249

[4] SKOLNIK, M. I. *Introduction to Radar System*. 3rd ed. Beaverton (OR, USA): McGraw-Hill, 2002. ISBN: 0072909803

[5] UYSAL, F. Comparison of range migration correction algorithms for range-Doppler processing. *Journal of Applied Remote Sensing*, 2017, vol. 11, no. 3, p. 1–10. DOI: 10.1117/1.JRS.11.036023

[6] ADDABBO, P., ORLANDO, D., RICCI, G. Adaptive radar detection of dim moving targets in presence of range migration. *IEEE Signal Processing Letters*, 2019, vol. 26, no. 10, p. 1461 to 1465. DOI: 10.1109/LSP.2019.2936650

[7] CARLSON, B. D., EVANS, E. D., WILSON, S. L. Search radar detection and track with the Hough transform. I. System concept. *IEEE Transactions on Aerospace and Electronic Systems*, 1994, vol. 30, no. 1, p. 102–108. DOI: 10.1109/7.250410

[8] ZENG, J., HE, Z. Detection of weak target for MIMO radar based on Hough transform. *Journal of Systems Engineering and Electronics*, 2009, vol. 20, no. 1, p. 76–80. ISSN: 1004–4132

[9] OVEIS, A. H., SEBT, M. A. Coherent method for ground-moving target indication and velocity estimation using Hough transform. *IET Radar, Sonar & Navigation*, 2017, vol. 11, no. 4, p. 646–655. DOI: 10.1049/iet-rsn.2016.0262

[10] CARRETERO-MOYA, J., GISMERO-MENOYO, J., ASENSIO-LOPEZ, A., et al. Application of the Radon transform to detect small-targets in sea clutter. *IET Radar, Sonar & Navigation*, 2009, vol. 3, no. 2, p. 155–166. DOI: 10.1049/iet-rsn:20080123

[11] ZHANG, X., LIAO, G., ZHU, S., et al. Geometry-information-aided efficient radial velocity estimation for moving target imaging and location based on Radon transform. *IEEE Transactions on Geoscience and Remote Sensing*, 2015, vol. 53, no. 2, p. 1105 to 1117. DOI: 10.1109/TGRS.2014.2334322

[12] HOU, L., SONG, H., ZHENG, M., et al. Fast moving target imaging and motion parameters estimation based on Radon transform and bi-directional approach. *IET Radar, Sonar & Navigation*, 2016, vol. 10, no. 6, p. 1013–1023. DOI: 10.1049/iet-rsn.2014.0567

[13] PERRY, R. P., DIPIETRO, R. C., FANTE, R. L. SAR imaging of moving targets. *IEEE Transactions on Aerospace and Electronic Systems*, 1999, vol. 35, no. 1, p. 188–200. DOI: 10.1109/7.745691

[14] ZHAO, Y., WANG, J., HUANG, L., et al. Low complexity Keystone transform without interpolation for dim moving target detection. In *Proceedings of 2011 IEEE CIE International Conference on Radar*. Chengdu (China), 2011, p. 1745–1748. DOI: 10.1109/CIE-Radar.2011.6159907

[15] SUN, Z., LI, X., YI, W., et al. Detection of weak maneuvering target based on Keystone transform and matched filtering process. *Signal Processing*, 2017, vol. 140, p. 127–138. DOI: 10.1016/j.sigpro.2017.05.013

[16] YU, W., LU, X., SU, W., et al. Coherent integration and detection algorithm for hypersonic target based on modified pulse compression and Keystone transform. *Electronics Letters*, 2021, vol. 57, no. 25, p. 989–991. DOI: 10.1049/ell2.12321

[17] YU, W., SU, W., GU, H., et al. Maneuvering target detection method based on Keystone transform and Radon local mapping sparse-modified Lv's Distribution. *Signal, Image and Video Processing*, 2023, vol. 17, p. 2771–2778. DOI: 10.1007/s11760-023-02494-2

[18] QU, X., SUN, X., LIU, F., et al. Moving target coherent integration method based on TRCM-KT for UAV-mounted through-the-wall radar. *IEEE Signal Processing Letters*, 2025, vol. 32, p. 1775–1779. DOI: 10.1109/LSP.2025.3561090

[19] XU, J., YU, J., PENG, Y. N., et al. Radon-Fourier transform for radar target detection, I: Generalized Doppler filter bank. *IEEE Transactions on Aerospace and Electronic Systems*, 2011, vol. 47, no. 2, p. 1186–1202. DOI: 10.1109/TAES.2011.5751251

[20] XU, J., YU, J., PENG, Y. N., et al. Radon-Fourier transform for radar target detection, (II): Blind speed sidelobe suppression. *IEEE Transactions on Aerospace and Electronic Systems*, 2011, vol. 47, no. 4, p. 2473–2489. DOI: 10.1109/TAES.2011.6034645

[21] YU, J., XU, J., PENG, Y. N., et al. Radon-Fourier transform for radar target detection (III): Optimality and fast implementations. *IEEE Transactions on Aerospace and Electronic Systems*, 2012, vol. 48, no. 2, p. 991–1004. DOI: 10.1109/TAES.2012.6178044

[22] RAO, X., TAO, H., SU, J., et al. Axis rotation MTD algorithm for weak target detection. *Digital Signal Processing*, 2014, vol. 26, p. 81–86. DOI: 10.1016/j.dsp.2013.12.003

[23] HUANG, X., ZHANG, Y., ZHANG, L., et al. Detection and fast motion parameter estimation for target with range walk effect based on new axis rotation moving target detection. *Digital Signal Processing*, 2022, vol. 120, p. 1–17. DOI: 10.1016/j.dsp.2021.103274

[24] HUSSAIN, M., AHMED, R., CHEEMA, H. M. Segmented Radon Fourier transform for long-time coherent radars. *IEEE Sensors Journal*, 2023, vol. 23, no. 9, p. 9582–9594. DOI: 10.1109/JSEN.2023.3260024

[25] LI, X., CUI, G., YI, W., et al. Sequence-reversing transform-based coherent integration for high-speed target detection. *IEEE Transactions on Aerospace and Electronic Systems*, 2017, vol. 53, no. 3, p. 1573–1580. DOI: 10.1109/TAES.2017.2668018

[26] LI, H., MA, D., WU, R. A low complexity algorithm for across range unit effect correction of the moving target via range frequency polynomial-phase transform. *Digital Signal Processing*, 2017, vol. 62, p. 176–186. DOI: 10.1016/j.dsp.2016.12.001

[27] PAN, J., ZHU, Q., BAO, Q., et al. Coherent integration method based on Radon-NUFFT for moving target detection using frequency agile radar. *Sensors*, 2020, vol. 20, no. 8, p. 1–14. DOI: 10.3390/s20082176

[28] CHEN, Q., LIU, J. H., FU, C. W., et al. Performance analysis and side lobe suppression in Radon-Fourier transform based on random pulse repetition interval. *Computer Modeling & New Technologies*, 2014, vol. 18, no. 11, p. 48–54.

[29] QIAN, C., FU, C., LIU, J., et al. Coherent integration based on random pulse repetition interval Radon-Fourier transform (in Chinese). *Journal of Electronics & Information Technology*, 2015, vol. 37, no. 5, p. 1085–1090. DOI: 10.11999/JEIT140818

[30] LIU, Q. H., NGUYEN, N. An accurate algorithm for nonuniform fast Fourier transforms (NUFFT's). *IEEE Microwave and Guided Wave Letters*, 1998, vol. 8, no. 1, p. 18–20. DOI: 10.1109/75.650975

[31] FOURMONT, K. Non-equispaced fast Fourier transforms with applications to tomography. *Journal of Fourier Analysis and Applications*, 2003, vol. 9, no. 5, p. 431–450. DOI: 10.1007/s00041-003-0021-1

[32] WEN, M., HOULIHAN, J. Application of the non-uniform Fourier transform to non-uniformly sampled Fourier transform spectrometers. *Optics Communications*, 2023, vol. 540, p. 1–12. DOI: 10.1016/j.optcom.2023.129491

About the Authors ...

Wenchao YU (corresponding author) was born in Jiangsu Province, China. He received his B.S. degree and Ph.D. degree from the School of Electronic and Optical Engineering, Nanjing University of Science and Technology, Nanjing, China, in 2014 and 2019, respectively. He is currently a lecturer in Nanjing University of Science and Technology. His main research interests include synthetic aperture radar (SAR), maneuvering target detection and time-frequency analysis.

Weimin SU was born in Jiangsu Province, China. He received his Ph.D. degree from Nanjing University of Science and Technology, Nanjing, China, in 1998. He is currently a Professor in Nanjing University of Science and Technology, a senior member of the Chinese Institute of Electronics, a member of the Signal Processing Society of China. His research interests include signal processing technology and advanced SAR systems.

Hong GU was born in Jiangsu Province, China. He received his M.S. degree from Nanjing University of Science and Technology, Jiangsu, China, in 1991, and the Ph.D. degree in Xidian University, Shanxi, China, in 1995. He is currently a Professor in Nanjing University of Science and Technology, a Chinese Institute of Electronics senior member, and a member of radar branch of the Jiang Electronic Society. His research interests include noise SAR, radar signal processing and information systems.